Effects of Annealing on Phase Transformation and Corrosion Mechanism of Severely Deformed $Al_{0.3}CoCrFeNi$ High-Entropy Alloy

Author: Fu-Yun Tsai[a], Alice Pandaleon[a], Sean O'Brien[a], Andrew Martin[a], Alana Pauls[a], Farhan Ishrak[a], Michael Lastovich[a], Md Jasim Uddin[a], Zengqing Zhuo[b], Jinghua Guo[b], Martin Mwangi Thuo[a], Rajeev Gupta[a], Rajarshi Banerjee[c], Elizabeth Kautz[d], Bharat Gwalani[a*]

[a]Materials Science and Engineering, North Carolina State University, Raleigh, NC, 27607, USA

[b]Lawrence Berkeley National Lab, Berkeley, CA, 94720, USA.

[c] Materials Science and Engineering, University of North Texas, Denton, USA

[d]Nuclear Engineering Department, North Carolina State University, Raleigh, North Carolina 27695, USA

Corresponding author: bgwalan@ncsu.edu (Bharat Gwalani)

Supplementary files:

1. Microstructure evolution during 620 °C annealing after 90% cold-rolling from 0 h to 50 h

Fig.S1 illustrates the SEM, EBSD, and TEM images of the $Al_{0.3}CoCrFeNi$ alloy subjected to 90% cold rolling followed by annealing at 620 °C for varying durations (0, 10, and 50 hours). The unannealed sample exhibits a heavily deformed structure with elongated grains, indicative of severe plastic deformation without new phase formation. SEM and EBSD images reveal a featureless texture with minimal contrast, while TEM images show high dislocation densities.

After 10 hours of annealing, grain boundary contrast becomes more pronounced, signaling the onset of recrystallization. Secondary phases such as B2 and sigma begin to precipitate, as shown in Fig.3. At 50 hours, the microstructure evolves into fully developed grains with well-defined precipitates located at grain boundaries and within grains.

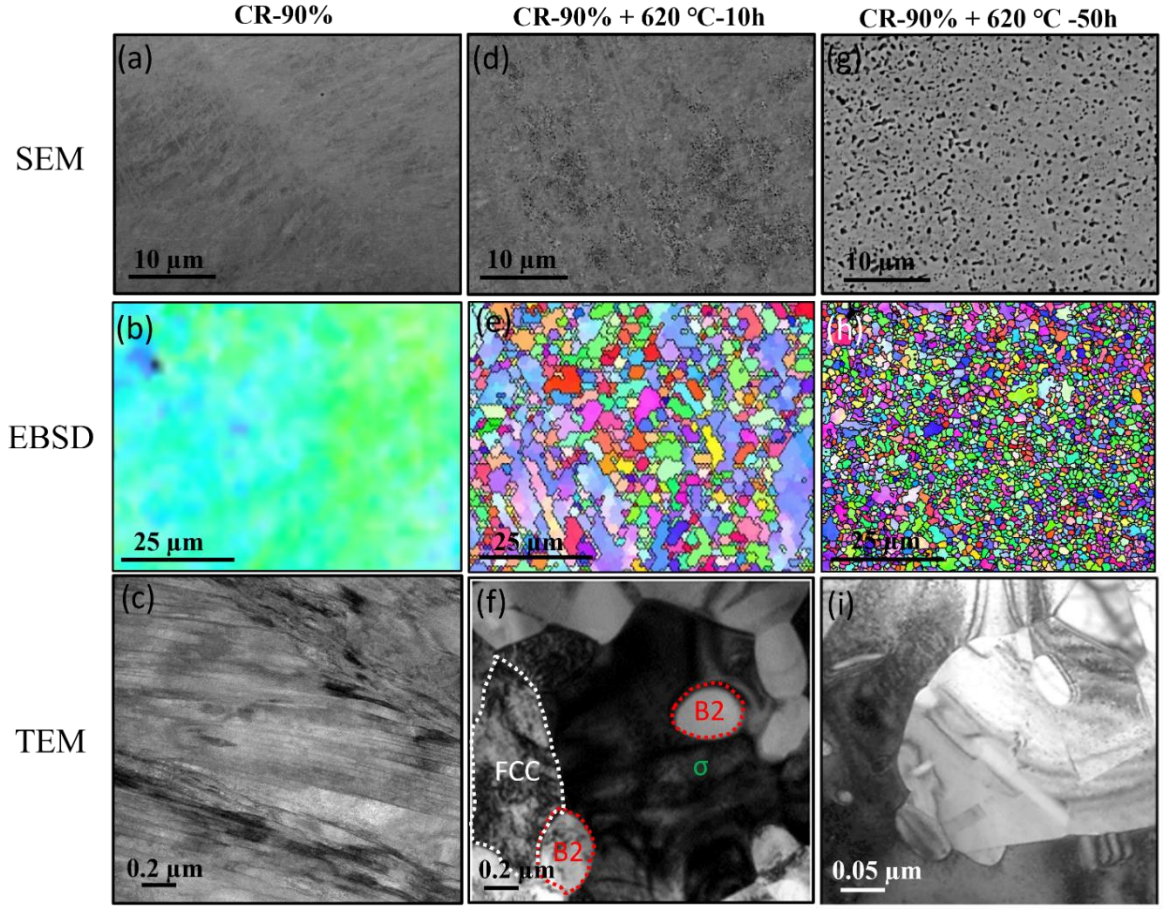

Fig. S1 Microstructural evolution during 620 °C annealing after 90 % cold-rolling:
(a–c) 0 h—severely deformed grains with high dislocation density;
(d–f) 10 h—partial recrystallisation and emergence of B2/σ precipitates;
(g–i) 50 h—fully recrystallised FCC matrix with coarsened intermetallics. Left to right: SEM, EBSD phase map, and TEM bright-field images, respectively.

As shown in Fig.S2, comparing the microstructures at 10h and 50h of annealing reveals significant phase evolution. At 10h, the material is predominantly FCC (90%), with minor Sigma

(8%) and Aluminum Nickel (2%). By 50h, a profound transformation occurs: FCC drops to 41%, while Sigma drastically increases to 45% (becoming dominant) and Aluminum Nickel rises to 15%. This shift is accompanied by a noticeable coarsening and segregation of phases.

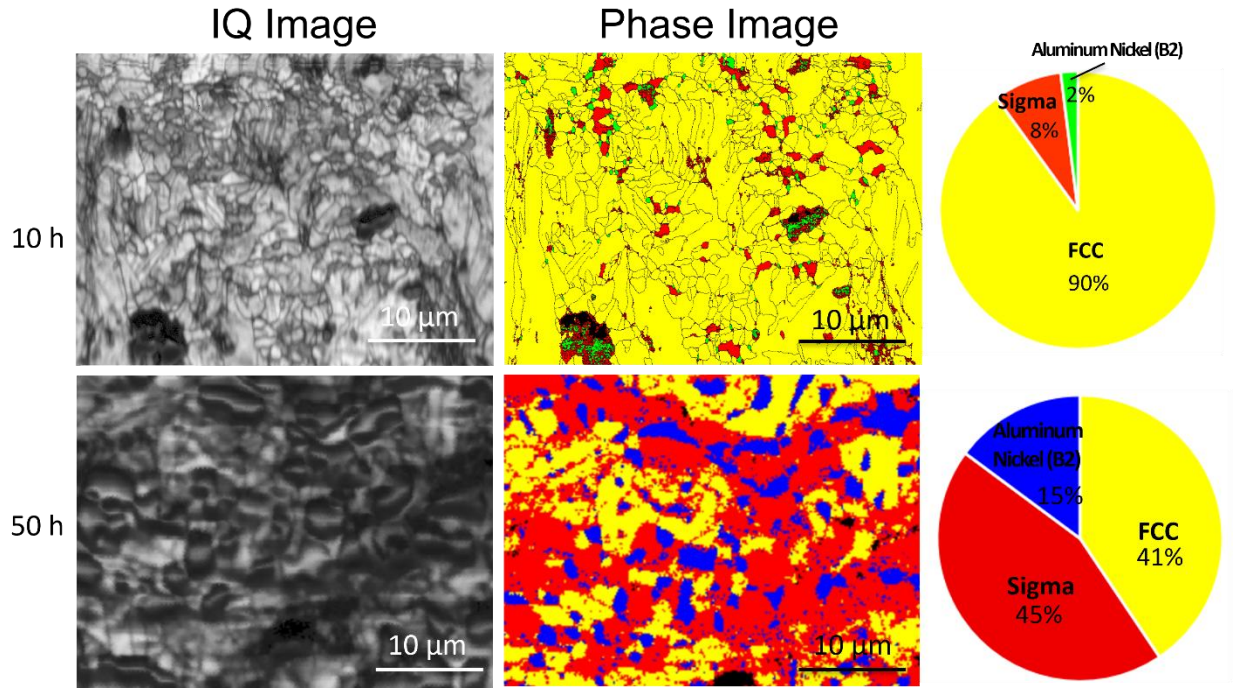

Fig.S2 EBSD IQ and Phase Images with Corresponding Phase Fractions after Annealing for 10 hours and 50 hours.

2. Microstrain data

The Williamson-Hall (W-H) method is a technique used to analyse micro-strain derived from X-ray diffraction. The Williamson-Hall equation is expressed as

$$\beta\cos(\theta)=K\lambda/L+4\epsilon\sin(\theta)$$

where β is the full width at half maximum (FWHM) of the diffraction peak (in radians)

θ is the Bragg angle of the diffraction peak

K is a constant related to the shape of the crystallites

λ is the X-ray wavelength

L is the crystallite size

ϵ is the microstrain

If we plot $\beta\cos(\theta)$ vs. $\sin(\theta)$, the slope should be four times the average microstrain in the crystal lattice.

As shown in Table.S1, annealing reduces microstrain and residual stresses caused by cold rolling. Prolonged annealing allows for the relaxation of defects, further contributing to a softer microstructure.

Table.S1 Micro-strain as function of treatment time

Treatment time at 620C after 90% CR	**Micro-strain**	**Error**
0	0.2616	0.0222
1	0.14	0.0163
2	0.1272	0.0178
4	0.1286	0.0225
16	0.1173	0.0193
50	0.1102	0.01364

Table.S2 shows lattice parameter as function of treatment time. For short annealing, precipitates like B2 or sigma phases begin to form, consuming solute atoms and reducing lattice distortion. This can decrease the lattice parameter. For longer annealing, further coarsening of precipitates and completion of phase transformations lead to a more stable matrix composition with a smaller lattice parameter.

Table.S2 Lattice parameter as function of treatment time

		Phase (Lattice parameter, Å)					
Condition	**time**	**FCC phase (a)**	**error**	**B2 Phase (a)**	**error**	**Sigma Phase (a, c)**	**error**
CR90	0	3.5928	0.0002				
CR90+620/1h	1	3.5871	0.0001				
CR90+620/2h	2	3.5863	0.0001				
CR90+620/4h	4	3.586	0.0002				
CR90+620/16h	16	3.5839	0.0001	2.875	0.001	8.7678, 4.55	0.008
CR90+620/50h	50	3.5804	0.0002	2.875	0.001	8.793, 4.548	0.004

Fig.S3 and Fig.S4 show the effects of cold work on the HEA alloy. Cold Working increases dislocation density and residual stresses, leading to higher microstrain.

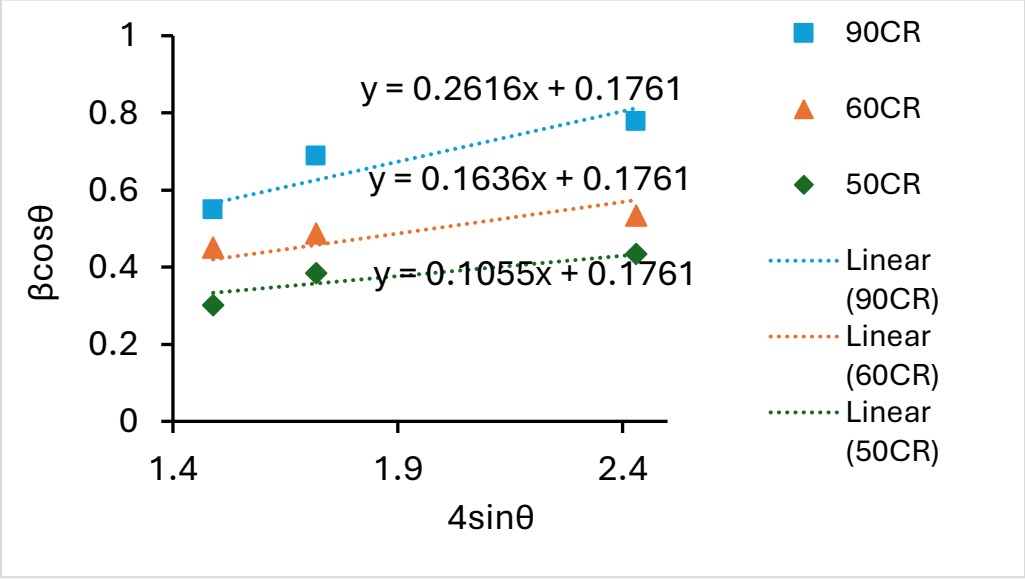

Fig.S3 Effect of cold work on the HEA alloy

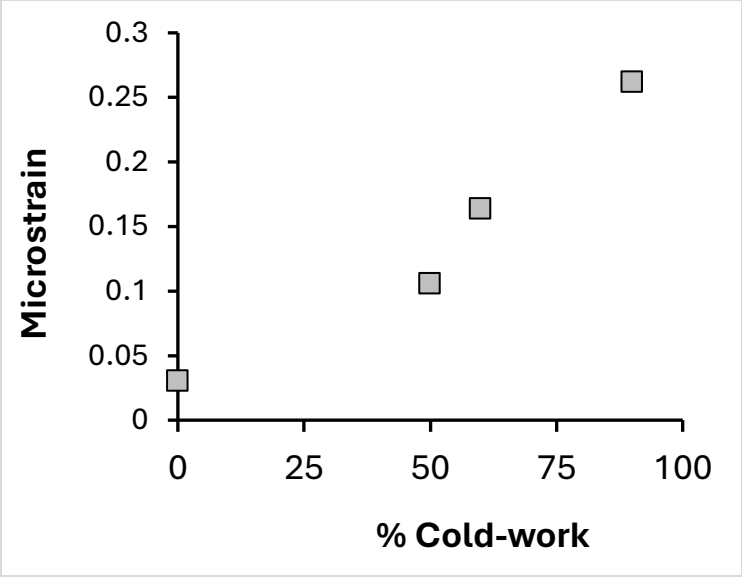

Fig.S4 Microstrain vs. cold work

3. XPS raw data

Fig.S5 presents XPS raw data for the Al 2p core levels of the base alloy and specimens annealed for different annealing times, all measured post-corrosion. The Al 2p spectra show a primary peak centered at approximately 74.4 eV, characteristic of aluminum oxide/hydroxide (Al^{3+}). This indicates that the corrosion layer on all samples is predominantly aluminum-rich. Across the base alloy and annealed samples, the peak position and shape remain largely consistent, suggesting that the chemical structure of the aluminum oxide layer is not significantly altered by annealing time.

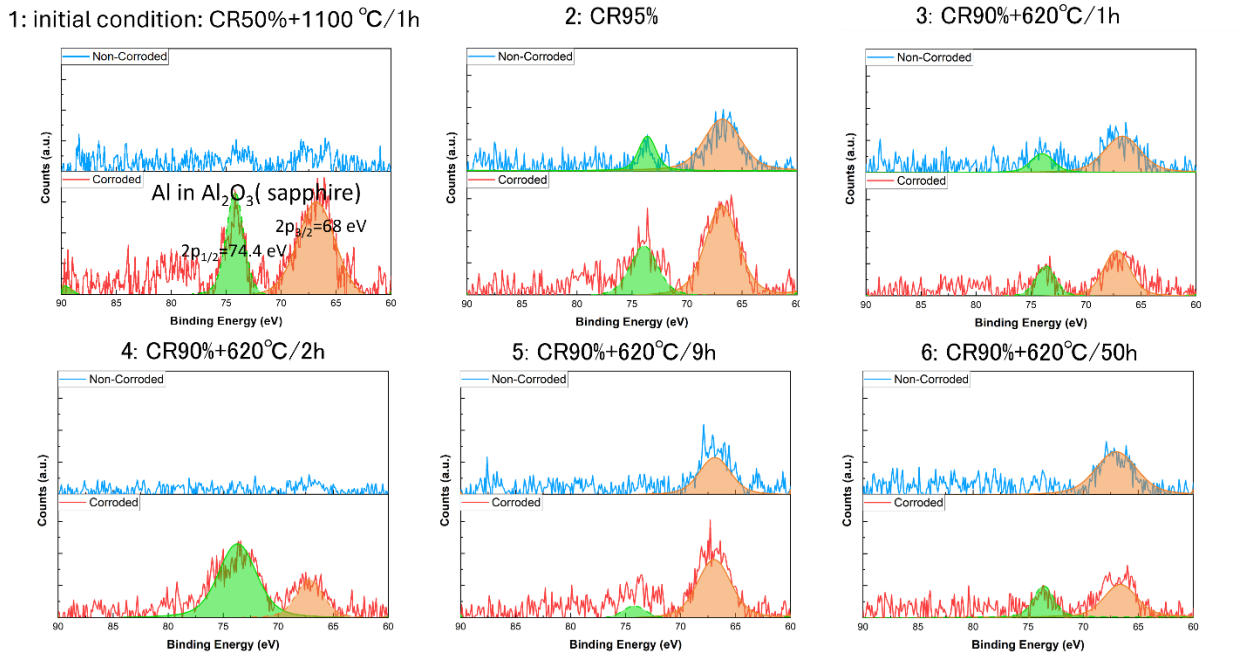

Fig.S5 XPS raw data of Al 2p peaks for the base alloy and specimens annealed 2 h and 50 h, post-corrosion.

Fig. S6 displays XPS raw data for the Cr $2p_{3/2}$ core levels of the base alloy and specimens annealed for different annealing times, post-corrosion. The spectra exhibit a distinct peak at approximately 586.7 eV, corresponding to trivalent chromium oxide (Cr^{3+}, e.g., Cr_2O_3). With increasing annealing time (base alloy < 2 h < 9 h), the intensity of the Cr^{3+} oxide peak increases,. This trend suggests that thermal treatment promotes the enrichment of protective chromium oxide in the passive layer, enhancing corrosion resistance.

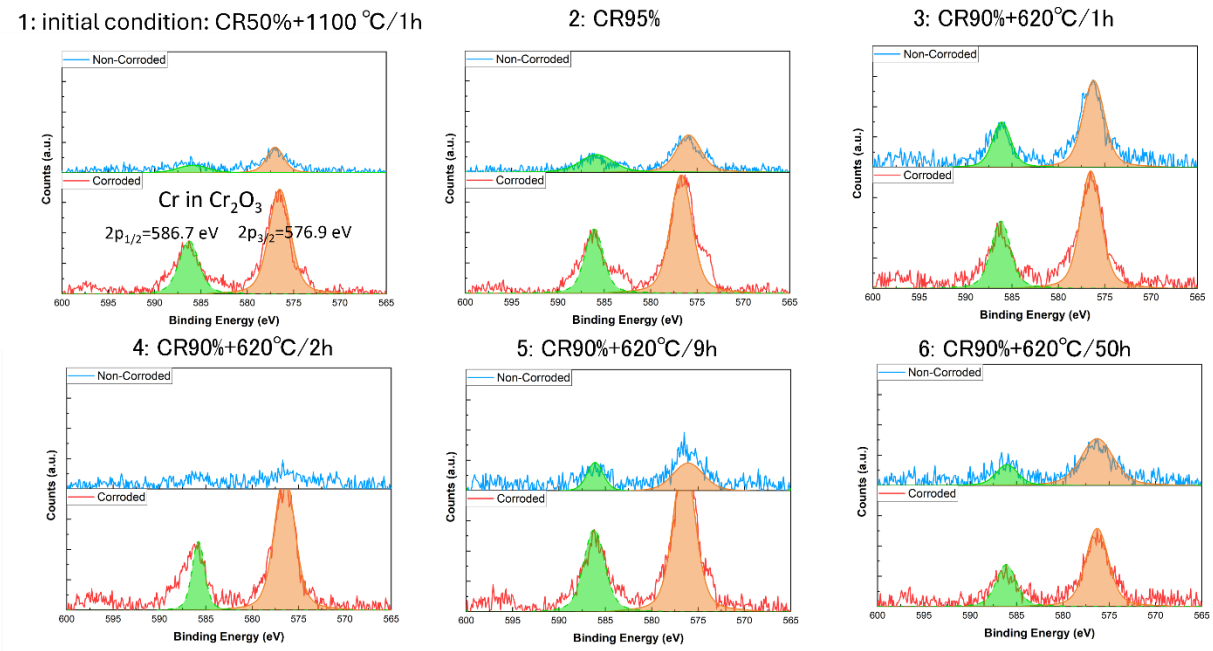

Fig.S6 XPS raw data of Cr $2p_{3/2}$ peaks for the base alloy and specimens annealed 2 h and 50 h, post-corrosion.